

Evidence for the singly-Cabibbo-suppressed decay $\Lambda_c^+ \rightarrow p\eta$ and search for $\Lambda_c^+ \rightarrow p\pi^0$

- M. Ablikim¹, M. N. Achasov^{9,e}, S. Ahmed¹⁴, X. C. Ai¹, O. Albayrak⁵, M. Albrecht⁴, D. J. Ambrose⁴⁵, A. Amoroso^{50A,50C}, F. F. An¹, Q. An^{47,a}, J. Z. Bai¹, O. Bakina²⁴, R. Baldini Ferroli^{20A}, Y. Ban³², D. W. Bennett¹⁹, J. V. Bennett⁵, N. Berger²³, M. Bertani^{20A}, D. Betttoni^{21A}, J. M. Bian⁴⁴, F. Bianchi^{50A,50C}, E. Boger^{24,c}, I. Boyko²⁴, R. A. Briere⁵, H. Cai⁵², X. Cai^{1,a}, O. Cakir^{41A}, A. Calcaterra^{20A}, G. F. Cao¹, S. A. Cetin^{41B}, J. Chai^{50C}, J. F. Chang^{1,a}, G. Chelkov^{24,c,d}, G. Chen¹, H. S. Chen¹, J. C. Chen¹, M. L. Chen^{1,a}, S. J. Chen³⁰, X. R. Chen²⁷, Y. B. Chen^{1,a}, X. K. Chu³², G. Cibinetto^{21A}, H. L. Dai^{1,a}, J. P. Dai^{35,j}, A. Dbeysi¹⁴, D. Dedovich²⁴, Z. Y. Deng¹, A. Denig²³, I. Denysenko²⁴, M. Destefanis^{50A,50C}, F. De Mori^{50A,50C}, Y. Ding²⁸, C. Dong³¹, J. Dong^{1,a}, L. Y. Dong¹, M. Y. Dong^{1,a}, O. Dorjkhaidav²², Z. L. Dou³⁰, S. X. Du⁵⁴, P. F. Duan¹, J. Z. Fan⁴⁰, J. Fang^{1,a}, S. S. Fang¹, X. Fang^{47,a}, Y. Fang¹, R. Farinelli^{21A,21B}, L. Fava^{50B,50C}, S. Fegan²³, F. Feldbauer²³, G. Felici^{20A}, C. Q. Feng^{47,a}, E. Fioravanti^{21A}, M. Fritsch^{14,23}, C. D. Fu¹, Q. Gao¹, X. L. Gao^{47,a}, Y. Gao⁴⁰, Z. Gao^{47,a}, I. Garzia^{21A}, K. Goetzen¹⁰, L. Gong³¹, W. X. Gong^{1,a}, W. Gradi²³, M. Greco^{50A,50C}, M. H. Gu^{1,a}, Y. T. Gu¹², A. Q. Guo¹, L. B. Guo²⁹, R. P. Guo¹, Y. P. Guo²³, Z. Haddadi²⁶, A. Hafner²³, S. Han⁵², X. Q. Hao¹⁵, F. A. Harris⁴³, K. L. He¹, X. Q. He⁴⁶, F. H. Heinsius⁴, T. Held⁴, Y. K. Heng^{1,a}, T. Holtmann⁴, Z. L. Hou¹, C. Hu²⁹, H. M. Hu¹, T. Hu^{1,a}, Y. Hu¹, G. S. Huang^{47,a}, J. S. Huang¹⁵, X. T. Huang³⁴, X. Z. Huang³⁰, Z. L. Huang²⁸, T. Hussain⁴⁹, W. Ikegami Andersson⁵¹, Q. Ji¹, Q. P. Ji¹⁵, X. B. Ji¹, X. L. Ji^{1,a}, L. W. Jiang⁵², X. S. Jiang^{1,a}, X. Y. Jiang³¹, J. B. Jiao³⁴, Z. Jiao¹⁷, D. P. Jin^{1,a}, S. Jin¹, T. Johansson⁵¹, A. Julin⁴⁴, N. Kalantar-Nayestanaki²⁶, X. L. Kang¹, X. S. Kang³¹, M. Kavatsyuk²⁶, B. C. Ke⁵, P. Kiese²³, R. Kliemt¹⁰, B. Kloss²³, O. B. Kolcu^{41B,h}, B. Kopf⁴, M. Kornicer⁴³, A. Kupsc⁵¹, W. Kühn²⁵, J. S. Lange²⁵, M. Lara¹⁹, P. Larin¹⁴, L. Lavezzi^{50C,1}, H. Leithoff²³, C. Leng^{50C}, C. Li⁵¹, Cheng Li^{47,a}, D. M. Li⁵⁴, F. Li^{1,a}, F. Y. Li³², G. Li¹, H. B. Li¹, H. J. Li¹, J. C. Li¹, Jin Li³³, K. Li³⁴, K. Li¹³, Lei Li³, P. L. Li^{47,a}, P. R. Li^{7,42}, Q. Y. Li³⁴, T. Li³⁴, W. D. Li¹, W. G. Li¹, X. L. Li³⁴, X. N. Li^{1,a}, X. Q. Li³¹, Z. B. Li³⁹, H. Liang^{47,a}, Y. F. Liang³⁷, Y. T. Liang²⁵, G. R. Liao¹¹, D. X. Lin¹⁴, B. Liu^{35,j}, B. J. Liu¹, C. X. Liu¹, D. Liu^{47,a}, F. H. Liu³⁶, Fang Liu¹, Feng Liu⁶, H. B. Liu¹², H. H. Liu¹, H. H. Liu¹⁶, H. M. Liu¹, J. B. Liu^{47,a}, J. P. Liu⁵², J. Y. Liu¹, K. Liu⁴⁰, K. Y. Liu²⁸, L. D. Liu³², P. L. Liu^{1,a}, Q. Liu⁴², S. B. Liu^{47,a}, X. Liu²⁷, Y. B. Liu³¹, Y. Y. Liu³¹, Z. A. Liu^{1,a}, Zhiqing Liu²³, H. Loehner²⁶, Y. F. Long³², X. C. Lou^{1,a,g}, H. J. Lu¹⁷, J. G. Lu^{1,a}, Y. Lu¹, Y. P. Lu^{1,a}, C. L. Luo²⁹, M. X. Luo⁵³, T. Luo⁴³, X. L. Luo^{1,a}, X. R. Lyu⁴², F. C. Ma²⁸, H. L. Ma¹, L. L. Ma³⁴, M. M. Ma¹, Q. M. Ma¹, T. Ma¹, X. N. Ma³¹, X. Y. Ma^{1,a}, Y. M. Ma³⁴, F. E. Maas¹⁴, M. Maggiore^{50A,50C}, Q. A. Malik⁴⁹, Y. J. Mao³², Z. P. Mao¹, S. Marcello^{50A,50C}, J. G. Messchendorp²⁶, G. Mezzadri^{21B}, J. Min^{1,a}, T. J. Min¹, R. E. Mitchell¹⁹, X. H. Mo^{1,a}, Y. J. Mo⁶, C. Morales Morales¹⁴, G. Morello^{20A}, N. Yu. Muchnoi^{9,e}, H. Muramatsu⁴⁴, P. Musiol⁴, Y. Nefedov²⁴, F. Nerling¹⁰, I. B. Nikolaev^{9,e}, Z. Ning^{1,a}, S. Nisar⁸, S. L. Niu^{1,a}, X. Y. Niu¹, S. L. Olsen³³, Q. Ouyang^{1,a}, S. Pacetti^{20B}, Y. Pan^{47,a}, P. Patteri^{20A}, M. Pelizaeus⁴, H. P. Peng^{47,a}, K. Peters^{10,i}, J. Pettersson⁵¹, J. L. Ping²⁹, R. G. Ping¹, R. Poling⁴⁴, V. Prasad¹, H. R. Qi², M. Qi³⁰, S. Qian^{1,a}, C. F. Qiao⁴², J. J. Qin⁴², N. Qin⁵², X. S. Qin¹, Z. H. Qin^{1,a}, J. F. Qiu¹, K. H. Rashid^{49,k}, C. F. Redmer²³, M. Ripka²³, G. Rong¹, Ch. Rosner¹⁴, X. D. Ruan¹², A. Sarantsev^{24,f}, M. Savrié^{21B}, C. Schnier⁴, K. Schoenning⁵¹, W. Shan³², M. Shao^{47,a}, C. P. Shen², P. X. Shen³¹, X. Y. Shen¹, H. Y. Sheng¹, J. J. Song³⁴, X. Y. Song¹, S. Sosio^{50A,50C}, S. Spataro^{50A,50C}, G. X. Sun¹, J. F. Sun¹⁵, S. S. Sun¹, X. H. Sun¹, Y. J. Sun^{47,a}, Y. Z. Sun¹, Z. J. Sun^{1,a}, Z. T. Sun¹⁹, C. J. Tang³⁷, X. Tang¹, I. Tapan^{41C}, E. H. Thorndike⁴⁵, M. Tiemens²⁶, I. Uman^{41D}, G. S. Varner⁴³, B. Wang¹, B. L. Wang⁴², D. Wang³², D. Y. Wang³², Dan Wang⁴², K. Wang^{1,a}, L. L. Wang¹, L. S. Wang¹, M. Wang³⁴, P. Wang¹, P. L. Wang¹, W. P. Wang^{47,a}, X. F. Wang⁴⁰, Y. D. Wang¹⁴, Y. F. Wang^{1,a}, Y. Q. Wang²³, Z. Wang^{1,a}, Z. G. Wang^{1,a}, Z. H. Wang^{47,a}, Z. Y. Wang¹, Z. Y. Wang¹, T. Weber²³, D. H. Wei¹¹, P. Weidenkaff²³, S. P. Wen¹, U. Wiedner⁴, M. Wolke⁵¹, L. H. Wu¹, L. J. Wu¹, Z. Wu^{1,a}, L. Xia^{47,a}, L. G. Xia⁴⁰, Y. Xia¹⁸, D. Xiao¹, H. Xiao⁴⁸, Z. J. Xiao²⁹, Y. G. Xie^{1,a}, Y. H. Xie⁶, X. A. Xiong¹, Q. L. Xiu^{1,a}, G. F. Xu¹, J. J. Xu¹, L. Xu¹, Q. J. Xu¹³, Q. N. Xu⁴², X. P. Xu³⁸, L. Yan^{50A,50C}, W. B. Yan^{47,a}, W. C. Yan^{47,a}, Y. H. Yan¹⁸, H. J. Yang^{35,j}, H. X. Yang¹, L. Yang⁵², Y. X. Yang¹¹, M. Ye^{1,a}, M. H. Ye⁷, J. H. Yin¹, Z. Y. You³⁹, B. X. Yu^{1,a}, C. X. Yu³¹, J. S. Yu²⁷, C. Z. Yuan¹, Y. Yuan¹, A. Yuncu^{41B,b}, A. A. Zafar⁴⁹, Y. Zeng¹⁸, Z. Zeng^{47,a}, B. X. Zhang¹, B. Y. Zhang^{1,a}, C. C. Zhang¹, D. H. Zhang¹, H. H. Zhang³⁹, H. Y. Zhang^{1,a}, J. Zhang¹, J. L. Zhang¹, J. Q. Zhang¹, J. W. Zhang^{1,a}, J. Y. Zhang¹, J. Z. Zhang¹, K. Zhang¹, S. Q. Zhang³¹, X. Y. Zhang³⁴, Y. Zhang¹, Y. Zhang¹, Y. H. Zhang^{1,a}, Y. N. Zhang⁴², Y. T. Zhang^{47,a}, Yu Zhang⁴², Z. H. Zhang⁶, Z. P. Zhang⁴⁷, Z. Y. Zhang⁵², G. Zhao¹, J. W. Zhao^{1,a}, J. Y. Zhao¹, J. Z. Zhao^{1,a}, Lei Zhao^{47,a}, Ling Zhao¹, M. G. Zhao³¹, Q. Zhao¹, S. J. Zhao⁵⁴, T. C. Zhao¹, Y. B. Zhao^{1,a}, Z. G. Zhao^{47,a}, A. Zhemchugov^{24,c}, B. Zheng^{14,48}, J. P. Zheng^{1,a}, W. J. Zheng³⁴, Y. H. Zheng⁴², B. Zhong²⁹, L. Zhou^{1,a}, X. Zhou⁵², X. K. Zhou^{47,a}, X. R. Zhou^{47,a}, X. Y. Zhou¹, K. Zhu¹, K. J. Zhu^{1,a}, S. Zhu¹, S. H. Zhu⁴⁶, X. L. Zhu⁴⁰, Y. C. Zhu^{47,a}, Y. S. Zhu¹, Z. A. Zhu¹, J. Zhuang^{1,a}, L. Zotti^{50A,50C}, B. S. Zou¹, J. H. Zou¹

(BESIII Collaboration)

- ¹ Institute of High Energy Physics, Beijing 100049, People's Republic of China
² Beihang University, Beijing 100191, People's Republic of China
³ Beijing Institute of Petrochemical Technology, Beijing 102617, People's Republic of China
⁴ Bochum Ruhr-University, D-44780 Bochum, Germany
⁵ Carnegie Mellon University, Pittsburgh, Pennsylvania 15213, USA
⁶ Central China Normal University, Wuhan 430079, People's Republic of China
⁷ China Center of Advanced Science and Technology, Beijing 100190, People's Republic of China
⁸ COMSATS Institute of Information Technology, Lahore, Defence Road, Off Raiwind Road, 54000 Lahore, Pakistan
⁹ G.I. Budker Institute of Nuclear Physics SB RAS (BINP), Novosibirsk 630090, Russia
¹⁰ GSI Helmholtzcentre for Heavy Ion Research GmbH, D-64291 Darmstadt, Germany
¹¹ Guangxi Normal University, Guilin 541004, People's Republic of China
¹² Guangxi University, Nanning 530004, People's Republic of China
¹³ Hangzhou Normal University, Hangzhou 310036, People's Republic of China
¹⁴ Helmholtz Institute Mainz, Johann-Joachim-Becher-Weg 45, D-55099 Mainz, Germany
¹⁵ Henan Normal University, Xinxiang 453007, People's Republic of China
¹⁶ Henan University of Science and Technology, Luoyang 471003, People's Republic of China
¹⁷ Huangshan College, Huangshan 245000, People's Republic of China
¹⁸ Hunan University, Changsha 410082, People's Republic of China
¹⁹ Indiana University, Bloomington, Indiana 47405, USA
²⁰ (A)INFN Laboratori Nazionali di Frascati, I-00044, Frascati, Italy; (B)INFN and University of Perugia, I-06100, Perugia, Italy
²¹ (A)INFN Sezione di Ferrara, I-44122, Ferrara, Italy; (B)University of Ferrara, I-44122, Ferrara, Italy
²² Institute of Physics and Technology, Peace Ave. 54B, Ulaanbaatar 13330, Mongolia
²³ Johannes Gutenberg University of Mainz, Johann-Joachim-Becher-Weg 45, D-55099 Mainz, Germany
²⁴ Joint Institute for Nuclear Research, 141980 Dubna, Moscow region, Russia
²⁵ Justus-Liebig-Universitaet Giessen, II. Physikalisches Institut, Heinrich-Buff-Ring 16, D-35392 Giessen, Germany
²⁶ KVI-CART, University of Groningen, NL-9747 AA Groningen, The Netherlands
²⁷ Lanzhou University, Lanzhou 730000, People's Republic of China
²⁸ Liaoning University, Shenyang 110036, People's Republic of China
²⁹ Nanjing Normal University, Nanjing 210023, People's Republic of China
³⁰ Nanjing University, Nanjing 210093, People's Republic of China
³¹ Nankai University, Tianjin 300071, People's Republic of China
³² Peking University, Beijing 100871, People's Republic of China
³³ Seoul National University, Seoul, 151-747 Korea
³⁴ Shandong University, Jinan 250100, People's Republic of China
³⁵ Shanghai Jiao Tong University, Shanghai 200240, People's Republic of China
³⁶ Shanxi University, Taiyuan 030006, People's Republic of China
³⁷ Sichuan University, Chengdu 610064, People's Republic of China
³⁸ Soochow University, Suzhou 215006, People's Republic of China
³⁹ Sun Yat-Sen University, Guangzhou 510275, People's Republic of China
⁴⁰ Tsinghua University, Beijing 100084, People's Republic of China
⁴¹ (A)Ankara University, 06100 Tandoğan, Ankara, Turkey; (B)İstanbul Bilgi University, 34060 Eyüp, İstanbul, Turkey; (C)Uludag University, 16059 Bursa, Turkey; (D)Near East University, Nicosia, North Cyprus, Mersin 10, Turkey
⁴² University of Chinese Academy of Sciences, Beijing 100049, People's Republic of China
⁴³ University of Hawaii, Honolulu, Hawaii 96822, USA
⁴⁴ University of Minnesota, Minneapolis, Minnesota 55455, USA
⁴⁵ University of Rochester, Rochester, New York 14627, USA
⁴⁶ University of Science and Technology Liaoning, Anshan 114051, People's Republic of China
⁴⁷ University of Science and Technology of China, Hefei 230026, People's Republic of China
⁴⁸ University of South China, Hengyang 421001, People's Republic of China
⁴⁹ University of the Punjab, Lahore-54590, Pakistan

⁵⁰ (A) University of Turin, I-10125, Turin, Italy; (B) University of Eastern Piedmont, I-15121, Alessandria, Italy; (C) INFN, I-10125, Turin, Italy
⁵¹ Uppsala University, Box 516, SE-75120 Uppsala, Sweden
⁵² Wuhan University, Wuhan 430072, People's Republic of China
⁵³ Zhejiang University, Hangzhou 310027, People's Republic of China
⁵⁴ Zhengzhou University, Zhengzhou 450001, People's Republic of China

^a Also at State Key Laboratory of Particle Detection and Electronics, Beijing 100049, Hefei 230026, People's Republic of China

^b Also at Bogazici University, 34342 Istanbul, Turkey

^c Also at the Moscow Institute of Physics and Technology, Moscow 141700, Russia

^d Also at the Functional Electronics Laboratory, Tomsk State University, Tomsk, 634050, Russia

^e Also at the Novosibirsk State University, Novosibirsk, 630090, Russia

^f Also at the NRC "Kurchatov Institute", PNPI, 188300, Gatchina, Russia

^g Also at University of Texas at Dallas, Richardson, Texas 75083, USA

^h Also at Istanbul Arel University, 34295 Istanbul, Turkey

ⁱ Also at Goethe University Frankfurt, 60323 Frankfurt am Main, Germany

^j Also at Key Laboratory for Particle Physics, Astrophysics and Cosmology, Ministry of Education; Shanghai Key Laboratory for Particle Physics and Cosmology; Institute of Nuclear and Particle Physics, Shanghai 200240, People's Republic of China

^k Also at Government College Women University, Sialkot-51310, Punjab, Pakistan.

(Dated: July 4, 2017)

We study the singly-Cabibbo-suppressed decays $\Lambda_c^+ \rightarrow p\eta$ and $\Lambda_c^+ \rightarrow p\pi^0$ using $\Lambda_c^+\bar{\Lambda}_c^-$ pairs produced by e^+e^- collisions at a center-of-mass energy of $\sqrt{s} = 4.6$ GeV. The data sample was collected by the BESIII detector at the BEPCII collider and corresponds to an integrated luminosity of 567 pb^{-1} . We find the first evidence for the decay $\Lambda_c^+ \rightarrow p\eta$ with a statistical significance of 4.2σ and measure its branching fraction to be $\mathcal{B}(\Lambda_c^+ \rightarrow p\eta) = (1.24 \pm 0.28(\text{stat.}) \pm 0.10(\text{syst.})) \times 10^{-3}$. No significant $\Lambda_c^+ \rightarrow p\pi^0$ signal is observed. We set an upper limit on its branching fraction $\mathcal{B}(\Lambda_c^+ \rightarrow p\pi^0) < 2.7 \times 10^{-4}$ at the 90% confidence level.

PACS numbers: 14.20.Lq, 13.30.Eg, 12.38.Qk

Weak decays of charmed baryons provide a unique testing ground for different theoretical models and approaches, *e.g.* the quark model approach to non-leptonic charm decays and Heavy Quark Effective Theory [1–7]. The charmed baryon ground state Λ_c^+ was first observed in 1979 [8, 9], but, compared to the rapid advances of charmed mesons, progress in the studies of the charmed baryons has been relatively slow due to a lack of experimental data and the additional difficulties of three constituent quarks in theoretical calculation. The accuracy of Λ_c^+ branching fractions (BFs) has long been poor for the Cabibbo-favoured (CF) decays, and even worse, with uncertainties at the 40% level, for the singly-Cabibbo-suppressed (SCS) decays [10]. As a consequence, it is neither possible to test the BFs predicted by different theoretical models, nor to determine the effects of final-state interactions (FSI). It is therefore essential to improve the accuracy of these BFs for Λ_c^+ decays and to search for new decay modes. The absolute BFs of twelve Λ_c^+ CF hadronic decay modes have been measured by the BESIII collaboration with much improved precision [11].

The SCS decays $\Lambda_c^+ \rightarrow p\eta$ and $p\pi^0$ have not yet been studied experimentally. These two decays proceed predominantly through internal W -emission and W -exchange diagrams, which are non-factorizable and

not subject to color and helicity suppression in charmed baryon decay. Some theoretical models [3, 4, 12, 13], predict the BFs of these two processes under different assumptions (the flavor SU(3) symmetry, FSI) obtaining different results. Therefore, measurements of these BFs will help us to understand the underlying dynamics of charmed baryon decays and distinguish between the different models. Furthermore, the ratio of BFs of these two decays, which is expected to be relatively insensitive to the values of input parameters in the theoretical calculation, is an excellent probe to distinguish between the different models.

In this Letter, we present the first experimental investigations of the SCS decays $\Lambda_c^+ \rightarrow p\eta$ and $p\pi^0$. We use a data sample of e^+e^- collisions at a center-of-mass (c.m.) energy of $\sqrt{s} = 4.6$ GeV [14] with an integrated luminosity of 567 pb^{-1} [15] collected by the BESIII [16] detector at the BEPCII [17] collider. Taking advantage of the excellent BESIII detector performance and the clean environment just above the mass threshold to produce $\Lambda_c^+\bar{\Lambda}_c^-$ pairs, a single-tag method, (*i.e.*, reconstruction of only one Λ_c in the $\Lambda_c^+\bar{\Lambda}_c^-$ pairs) is used to increase the detection efficiency and acquire more Λ_c candidates. Throughout the text, the charge conjugate states are always implied unless mentioned explicitly.

BESIII [16] is a cylindrical spectrometer, consisting of a small-celled, Helium-based main drift chamber (MDC), a plastic scintillator Time-of-Flight system (TOF), a CsI(Tl) electromagnetic calorimeter (EMC), a superconducting solenoid providing a 1.0 T magnetic field, and a muon counter. The charged particle momentum resolution is 0.5% at a transverse momentum of 1 GeV/c and the photon energy resolution in the EMC is 2.5% (5%) in the barrel (endcap) region for 1 GeV photons. A more detailed description of the BESIII detector is given in Ref. [16].

High-statistics e^+e^- annihilation Monte Carlo (MC) samples, generated by the GEANT4-based [18, 19] MC simulation package BOOST [20], are used to investigate the backgrounds, to optimize the selection criteria, and to determine the detection efficiencies. The e^+e^- annihilation is simulated by the MC generator KKMC [21], taking into consideration the spread of the beam energy and the effect of the initial-state radiation (ISR). Inclusive MC samples, consisting of $\Lambda_c^+\bar{\Lambda}_c^-$ events, charmed meson $D_{(s)}^{(*)}$ pair production, ISR returns to lower mass charmonium(-like) ψ states, and continuum QED processes $e^+e^- \rightarrow q\bar{q}$ ($q = u, d, s$), are used to study the backgrounds. All known decay modes are generated with EVTGEN [22, 23] with BFs being the values of the Particle Data Group (PDG) [10], and the remaining unknown decay modes are generated by LUNDCHARM [24]. The signal MC samples of $e^+e^- \rightarrow \Lambda_c^+\bar{\Lambda}_c^-$ are produced with one Λ_c decaying to the final states of interest, $p\eta$ or $p\pi^0$, and the other Λ_c decaying generically to any of the possible final states.

Charged tracks, reconstructed from hits in the MDC, are required to have a polar angle θ satisfying $|\cos\theta| < 0.93$ and a point of closest approach to the interaction point within ± 10 cm along the beam direction (V_z) and 1 cm in the plane perpendicular to the beam (V_r). Information from the TOF is combined with the ionization energy loss (dE/dx) from the MDC to calculate particle identification (PID) confidence levels (C.L.) for the π , K , and p hypotheses. The mass hypothesis with the highest PID C.L. is assigned to each track. A further requirement $V_r < 0.2$ cm is imposed on the proton candidates to avoid backgrounds from beam interactions with residual gas inside the beam pipe and materials of beam pipe and MDC inner wall. Photon candidates are reconstructed by clustering energy deposits in the EMC crystals. Good photon candidates are required to have energies larger than 25 MeV in the barrel region ($|\cos\theta| < 0.8$) or 50 MeV in the endcap region ($0.86 < |\cos\theta| < 0.92$). To eliminate showers produced by charged particles, showers are required to be separated by more than 20° from anti-protons, and by more than 8° from other charged particles. The EMC time is required to be within (0, 700) ns of the event start time to suppress electronic noise and showers unrelated to the event [11]. The EMC shower shape variables are used to distinguish photons from anti-neutrons: the photon candidates are required to have a lateral moment [25] less than 0.4, and $E_{3\times 3}/E_{5\times 5}$ larger than 0.85, where the

$E_{3\times 3}$ ($E_{5\times 5}$) is the shower energies summed over 3×3 (5×5) crystals around the center of the shower.

In the studies of $\Lambda_c^+ \rightarrow p\eta$ and $\Lambda_c^+ \rightarrow p\pi^0$ decays, the η mesons are reconstructed in their two most prominent decay modes, $\eta \rightarrow \gamma\gamma$ ($\eta_{\gamma\gamma}$) and $\eta \rightarrow \pi^+\pi^-\pi^0$ ($\eta_{\pi^+\pi^-\pi^0}$), while the π^0 meson is reconstructed in its dominant decay mode $\pi^0 \rightarrow \gamma\gamma$. Candidate $\eta \rightarrow \gamma\gamma$ and $\pi^0 \rightarrow \gamma\gamma$ decays are selected using all $\gamma\gamma$ combinations with an invariant mass within 3 times the mass resolution (10 (6) MeV/c^2 for the η (π^0) signal) of their nominal masses (M_η or M_{π^0}) [10]. An additional requirement, $|\cos\theta_{\text{decay}}| < 0.9$, where θ_{decay} is the polar angle of one γ in the helicity frame of the $\gamma\gamma$ system, is imposed on the candidate $\eta \rightarrow \gamma\gamma$ decay to suppress combinatorial backgrounds. To improve the momentum resolution, the $\gamma\gamma$ invariant mass is then constrained to M_η or M_{π^0} mass, and the resultant momenta are used in the subsequent analysis. The candidate $\eta \rightarrow \pi^+\pi^-\pi^0$ are reconstructed using all $\pi^+\pi^-\pi^0$ combinations with an invariant mass satisfying $|M_{\pi^+\pi^-\pi^0} - M_\eta| < 12\text{MeV}/c^2$.

The Λ_c^+ is reconstructed using all combinations of the selected proton and the $\eta(\pi^0)$ candidates. For e^+e^- annihilation at $\sqrt{s} = 4.6\text{ GeV}$, there are no additional hadrons produced with the $\Lambda_c^+\bar{\Lambda}_c^-$ pair due to the limited phase space. Thus, two kinematic variables, the beam energy constrained mass $M_{\text{BC}} \equiv \sqrt{E_{\text{beam}}^2/c^4 - |\vec{p}_{\Lambda_c^+}|^2/c^2}$ and the energy difference $\Delta E \equiv E_{\Lambda_c^+} - E_{\text{beam}}$, are used to identify Λ_c^+ candidates. Here, $\vec{p}_{\Lambda_c^+}$ and $E_{\Lambda_c^+}$ are the reconstructed momentum and energy of the Λ_c^+ candidate in the e^+e^- c.m. system, and E_{beam} is the energy of the electron and positron beams. For a Λ_c^+ candidate that is reconstructed correctly, M_{BC} and ΔE are expected to be consistent with the Λ_c^+ nominal mass and zero, respectively. A Λ_c^+ candidate is accepted if the corresponding $|\Delta E|$ is less than 2.5 times its resolution ($\sigma_{\Delta E}$). The decay mode dependent ΔE requirements, are summarized in Table I. For a given decay mode, we accept at most one charmed baryon candidate per event, retaining the one with the minimum $|\Delta E|$. If there are candidates from different decay modes, we keep them all. For the decay mode $\Lambda_c^+ \rightarrow p\eta_{\pi^+\pi^-\pi^0}$, the peaking background from the CF decay mode $\Lambda_c^+ \rightarrow \pi^+\pi^-\Sigma^+(\Sigma^+ \rightarrow p\pi^0)$ is eliminated by requiring the invariant mass of proton and π^0 satisfying $|M_{p\pi^0} - M_{\Sigma^+}| > 0.015\text{GeV}/c^2$. The MC study shows that the residual peaking backgrounds from $\Lambda_c^+ \rightarrow \pi^+\pi^-\Sigma^+(\Sigma^+ \rightarrow p\pi^0)$ and from $\Lambda_c^+ \rightarrow \Lambda\pi^+\pi^0(\Lambda \rightarrow p\pi^-)$ and $\Lambda_c^+ \rightarrow pK_S^0\pi^0(K_S^0 \rightarrow \pi^+\pi^-)$, which have exactly the same final states as the signal, are negligible.

The resultant M_{BC} distributions for the decays $\Lambda_c^+ \rightarrow p\eta$ and $\Lambda_c^+ \rightarrow p\pi^0$ are depicted in Fig. 1 and Fig. 2, respectively. The $\Lambda_c^+ \rightarrow p\eta$ signals are seen in both η decay modes, but no obvious $\Lambda_c^+ \rightarrow p\pi^0$ signal is observed. The data in the ΔE sideband region, defined as $3.5\sigma_{\Delta E} < |\Delta E| < 6\sigma_{\Delta E}$, are used to study the backgrounds. The corresponding M_{BC} distributions, illustrated by the long-dashed histograms in Fig. 1 and Fig. 2, show no Λ_c^+ signal and that the combinatorial backgrounds are well

described by the data in the ΔE sideband region. For the decay mode $\Lambda_c^+ \rightarrow p\eta_{\pi^+\pi^-\pi^0}$, data in the η sideband region ($0.016 < |M_{\pi^+\pi^-\pi^0} - M_\eta| < 0.032$ GeV/c 2), illustrated by the (pink) dashed histogram in Fig. 1(b), also shows no evidence for peaking background. This is further validated by an analysis of the inclusive MC samples, where it is found that the combinatorial backgrounds are dominated by the processes $e^+e^- \rightarrow q\bar{q}$.

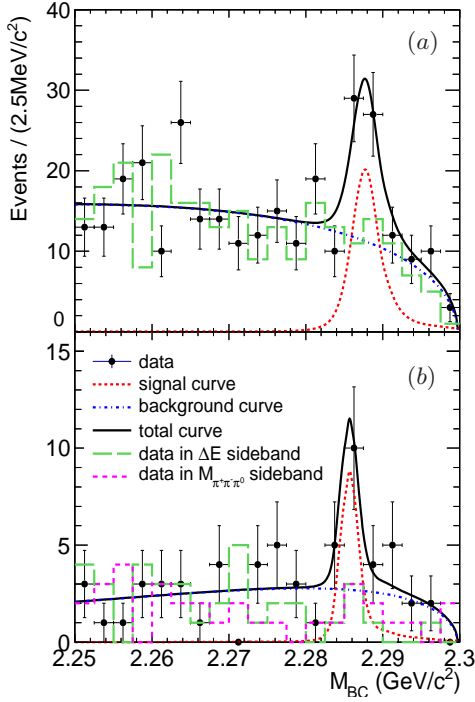


FIG. 1. (color online) Simultaneous fit to the M_{BC} distributions of $\Lambda_c^+ \rightarrow p\eta$ reconstructed with the decay modes (a) $\eta \rightarrow \gamma\gamma$ and (b) $\eta \rightarrow \pi^+\pi^-\pi^0$. The dots with error bars are data, the (black) solid curves are for the best fits, the (blue) dash-dotted curves are for the backgrounds, and the (red) dashed curves are for the signals. The (green) long-dashed histograms and (pink) dashed histogram (in (b) only) are the data in the ΔE and $M_{\pi^+\pi^-\pi^0}$ sideband region.

To extract the signal yield for the decay $\Lambda_c^+ \rightarrow p\eta$, we perform unbinned maximum likelihood fits to the M_{BC} distributions. The signal probability density function (PDF) is constructed by the signal MC simulated shape convoluted with a Gaussian function. Since MC simulation may be imperfect for modeling of the detector resolution and beam-energy spread of data, the mean and width of Gaussian function are free parameters to account for the potential mass shift and resolution difference between data and MC simulation. The mean (μ) and width (σ) values of Gaussian function are $\mu = (0.74 \pm 0.56)$ MeV/c 2 and $\sigma = (0.32 \pm 2.28)$ MeV/c 2 for $\Lambda_c^+ \rightarrow p\eta_{\gamma\gamma}$, while $\mu = (-1.22 \pm 0.80)$ MeV/c 2 and $\sigma = (0.02 \pm 1.44)$ MeV/c 2 for $\Lambda_c^+ \rightarrow p\eta_{\pi^+\pi^-\pi^0}$, respectively. The background shape is modeled by an AR-

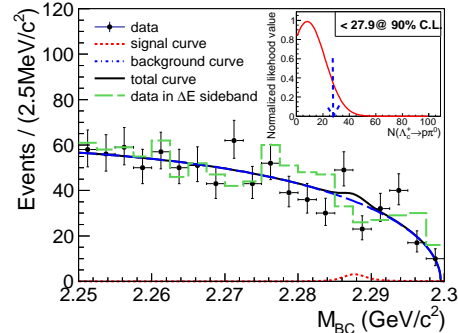


FIG. 2. (color online) Fit to the M_{BC} distribution for the decay $\Lambda_c^+ \rightarrow p\pi^0$. The dots with error bars are data, the (black) solid curve is for the best fit, and the (blue) dashed curve is for the background. The (green) long-dashed histogram is the data in the ΔE sideband region. The insert shows the normalized likelihood distribution, which includes the systematic uncertainty, as a function of the expected signal yield. The (blue) dashed arrow indicates the upper limit on the signal yield at 90% C.L.

GUS function [26] with the fixed high-end cutoff E_{beam} . The reliability of the ARGUS function is validated with the data in the ΔE sideband region as well as the inclusive MC samples in the signal region. In the decay $\Lambda_c^+ \rightarrow p\eta_{\pi^+\pi^-\pi^0}$, the peaking backgrounds from the CF decays have been found to be negligible by MC studies, and are not considered in the fit. The fits are performed for the two η decay modes separately. The corresponding BFs are calculated using

$$\mathcal{B}(\Lambda_c^+ \rightarrow p\eta) = \frac{N_{sig}}{2 \cdot N_{\Lambda_c^+ \bar{\Lambda}_c^-} \cdot \varepsilon \cdot \mathcal{B}_{inter}}, \quad (1)$$

where N_{sig} is the signal yield determined from the M_{BC} fit, $N_{\Lambda_c^+ \bar{\Lambda}_c^-} = (105.9 \pm 4.8(\text{stat.}) \pm 0.5(\text{syst.})) \times 10^3$ is the total number of $\Lambda_c^+ \bar{\Lambda}_c^-$ pairs in the data [11], ε is the detection efficiency estimated by the MC simulation, and \mathcal{B}_{inter} is the η or π^0 decay BF taken from the PDG [10]. The factor of 2 in the denominator accounts for the charge conjugation of the Λ_c^+ . Table I summarizes the signal yields, the statistical significances, estimated by the changes in the likelihood values obtained with and without the Λ_c^+ signal included, the detection efficiencies, and the resulting BFs. The two BFs for $\Lambda_c^+ \rightarrow p\eta$, corresponding to the two η decay modes, are consistent within statistical uncertainties.

We also perform a simultaneous fit to the M_{BC} distributions for the two η decay modes, constrained to the same $\mathcal{B}(\Lambda_c^+ \rightarrow p\eta)$ and taking into account the different detection efficiencies and decay BFs of η . The projections of the fit curves are illustrated in Fig. 1. In the fit, the likelihood values of the two individual η decay modes are calculated as a function of BF, and are smeared by considering the correlated and uncorrelated systematic uncertainties (discussed in detail below) between the two η decay modes according to Refs. [27, 28]. The overall

TABLE I. Summary of the ΔE signal regions, the signal yields, the statistical significances, the detection efficiencies, and the BFs (where the first uncertainties are statistical, and the second systematic) for the different Λ_c^+ decay modes.

	$p\eta_{\gamma\gamma}$	$p\eta_{\pi^+\pi^-\pi^0}$	$p\pi^0$
ΔE (GeV)	$[-0.034, 0.030]$	$[-0.027, 0.018]$	$[-0.056, 0.029]$
N_{sig}	38 ± 11	14 ± 5	< 27.9
Significance	3.2σ	2.7σ	...
$\epsilon(\%)$	39.8	20.3	49.0
$\mathcal{B}(\times 10^{-3})$	$1.15 \pm 0.33 \pm 0.10$	$1.45 \pm 0.52 \pm 0.15$	< 0.27

likelihood value in the fit is the product of those for the two η decay modes. The resultant BF is determined to be $\mathcal{B}(\Lambda_c^+ \rightarrow p\eta) = (1.24 \pm 0.28(\text{stat.}) \pm 0.10(\text{syst.})) \times 10^{-3}$ with a statistical significance of 4.2σ , where the significance is estimated by the difference of maximum likelihood values for simultaneous fits with and without signal.

Since no significant $\Lambda_c^+ \rightarrow p\pi^0$ signal is observed, an upper limit on the BF is estimated. We fit the M_{BC} distribution for the candidate $\Lambda_c^+ \rightarrow p\pi^0$ events using similar signal and background shapes to those described previously. The result of the best fit is shown in Fig. 2. For the signal PDF, the MC shape is convoluted with a Gaussian function with parameters fixed to those obtained in the fit to $\Lambda_c^+ \rightarrow p\eta_{\gamma\gamma}$ candidates. The PDF for the expected signal yield is taken to be the normalized likelihood \mathcal{L} obtained by scanning over the signal yield fixed from zero to a large number, and incorporating systematic uncertainties [27, 28], as shown in the inset plot of Fig. 2. The upper limit at the 90% C.L. on the signal yield is $N^{\text{up}} = 27.9$ (shown as the arrow in Fig. 2), corresponding to $\int_0^{N^{\text{up}}} \mathcal{L}(x) dx / \int_0^\infty \mathcal{L}(x) dx = 0.9$. The upper limit at the 90% C.L. on the BF is calculated with Eq. (1) by substituting η with π^0 and is reported in Table I.

Several sources of systematic uncertainties are considered in the BF measurements. The uncertainties associated with the efficiencies of the tracking and PID for charged tracks are investigated with the samples $e^+e^- \rightarrow 2(\pi^+\pi^-)$, $K^+K^-\pi^+\pi^-$ and $p\bar{p}\pi^+\pi^-$ from data taken at $\sqrt{s} > 4.0$ GeV, and the corresponding (transverse) momentum weighted values are assigned as the uncertainties. The uncertainties due to the V_r requirement and the veto on the CF peaking background in the decay $\Lambda_c^+ \rightarrow p\eta_{\pi^+\pi^-\pi^0}$ are investigated by repeating the analysis with alternative requirements ($V_r < 0.25$ cm and $|M_{p\pi^0} - M_{\Sigma^+}| > 0.020$ GeV/c 2). The resultant differences of the BFs are taken as the systematic uncertainties. The π^0 reconstruction efficiency, including the photon detection efficiency, is studied using a control sample of $D^0 \rightarrow K^-\pi^+\pi^0$ events from a data sample taken at $\sqrt{s} = 3.773$ GeV. The momentum weighted data-MC differences of the π^0 reconstruction efficiencies, which are obtained to be 3.3% and 0.8% for $\Lambda_c^+ \rightarrow p\eta_{\pi^+\pi^-\pi^0}$ and $\Lambda_c^+ \rightarrow p\pi^0$ decays, are considered as the uncertainties. Similarly, the uncertainty for the $\eta_{\gamma\gamma}$ reconstruction efficiency in the decay $\Lambda_c^+ \rightarrow p\eta_{\gamma\gamma}$ is determined to be 1.0%

by assuming the same momentum-dependent data-MC differences as those for π^0 candidates. The uncertainties associated with the η mass window for $\Lambda_c^+ \rightarrow p\eta_{\pi^+\pi^-\pi^0}$, the $\cos\theta_{\text{decay}}$ requirement for $\Lambda_c^+ \rightarrow p\eta_{\gamma\gamma}$, the ΔE requirements, and the photon shower requirements are studied using double-tag $D^+ \rightarrow \pi^+\eta(\pi^0)$ events. The uncertainties from the M_{BC} fit for $\Lambda_c^+ \rightarrow p\eta$ candidates are studied by alternative fits with different signal shapes, background parameters, and fit ranges, and the resultant changes on the BFs are taken as the uncertainties. In the determination of the upper limit on the BF of $\Lambda_c^+ \rightarrow p\pi^0$ decay, similar alternative fits are investigated, and the one corresponding to the largest upper limit is selected conservatively. The uncertainties in the signal MC model arising from the following sources are considered: a) the beam energy spread; b) the input cross section line-shape of $e^+e^- \rightarrow \Lambda_c^+\bar{\Lambda}_c^-$ production for ISR; c) the Λ_c^+ polar angle distribution in the e^+e^- rest frame; d) the different angular momentum between proton and $\eta(\pi^0)$ candidates. The quadratic sum of the resultant differences in the detection efficiencies is taken as the uncertainty. The uncertainties of the MC statistics, the total $\Lambda_c^+\bar{\Lambda}_c^-$ number quoted from Ref. [11] and the decay BFs for the intermediate state decays quoted from the PDG [10] are also considered. The total systematic uncertainties, quadratic sum of the individual ones, are 8.3%, 10.2%, and 5.2% for $\Lambda_c^+ \rightarrow p\eta_{\gamma\gamma}$, $p\eta_{\pi^+\pi^-\pi^0}$ and $p\pi^0$, respectively. The individual systematic uncertainties are summarized in the Table II.

TABLE II. Summary of the relative systematic uncertainties in percent for $\Lambda_c^+ \rightarrow p\eta_{\gamma\gamma}$, $p\eta_{\pi^+\pi^-\pi^0}$ and $p\pi^0$. The sources tagged with '*' are 100% correlated between the two η decay modes.

Sources	$p\eta_{\gamma\gamma}$	$p\eta_{\pi^+\pi^-\pi^0}$	$p\pi^0$
*Tracking for p	1.3	1.3	1.3
*PID for p	0.3	0.3	0.3
Tracking for $\pi^+\pi^-$...	2.0	...
PID for $\pi^+\pi^-$...	2.0	...
* V_r requirement	0.2	0.2	0.2
CF peaking background veto	...	1.3	...
$\eta_{\gamma\gamma}/\pi^0$ reconstruction	1.0	3.3	0.8
$M_{\pi^+\pi^-\pi^0}$ mass window	...	1.2	...
$\cos\theta_{\text{decay}}$ requirement	1.2
ΔE requirement	0.4	1.5	0.4
Shower requirement	0.8	1.9	1.7
M_{BC} fit	6.5	7.1	...
Signal MC model	0.7	1.2	0.8
MC statistics	0.1	0.1	0.1
* $N_{\Lambda_c^+\bar{\Lambda}_c^-}$	4.6	4.6	4.6
$\mathcal{B}_{\text{inter}}$	0.5	1.2	negligible
Total	8.3	10.2	5.2

In summary, using 567 pb^{-1} of e^+e^- annihilation data taken at a c.m. energy of $\sqrt{s} = 4.6$ GeV with the BE-SIII detector, we find the first evidence for the SCS decay $\Lambda_c^+ \rightarrow p\eta$ with a statistical significance of 4.2σ and measure its absolute BF to be $\mathcal{B}(\Lambda_c^+ \rightarrow p\eta) = (1.24 \pm 0.28(\text{stat.}) \pm 0.10(\text{syst.})) \times 10^{-3}$. In a search for the

SCS decay $\Lambda_c^+ \rightarrow p\pi^0$, no obvious signal is observed and an upper limit at the 90% C.L. on its BF is determined to be $\mathcal{B}(\Lambda_c^+ \rightarrow p\pi^0) < 2.7 \times 10^{-4}$. The corresponding ratio of BFs between the two decays is also calculated to be $\mathcal{B}(\Lambda_c^+ \rightarrow p\pi^0)/\mathcal{B}(\Lambda_c^+ \rightarrow p\eta) < 0.24$, where the common uncertainties are cancelled. The measured BFs and their ratio are compared to the theoretical predictions from different models, as shown in Table III. Our measured BF of $\Lambda_c^+ \rightarrow p\eta$ is consistent, within two standard deviations, with one of predictions in Ref. [3], the one that assumes flavor SU(3) symmetry and negative sign for p-wave amplitude of $\Lambda_c^+ \rightarrow \Xi^0 K^+$. It is worth noting that our measurement is significantly higher than other's theoretical predictions. The measured upper limit of $\mathcal{B}(\Lambda_c^+ \rightarrow p\pi^0)$ is compatible with the predicted values of most of theoretical models, but is smaller by a factor of 2 than that in Ref. [13]. Overall, the obtained relatively large value of $\mathcal{B}(\Lambda_c^+ \rightarrow p\eta)$ and the trend toward small value of the ratio $\mathcal{B}(\Lambda_c^+ \rightarrow p\pi^0)/\mathcal{B}(\Lambda_c^+ \rightarrow p\eta)$ will have a significant impact on theoretical calculation and will be helpful to understand the underlying dynamics of charmed baryon decays and to test SU(3) flavor symmetry. Additional experimental data will improve the sensitivity of the measurements and allow a better discrimination between the different models.

TABLE III. Comparison of measured BFs (in 10^{-3}) of $\Lambda_c^+ \rightarrow p\eta$ and $p\pi^0$ and their ratio to theoretical predictions.

	$\Lambda_c^+ \rightarrow p\eta$	$\Lambda_c^+ \rightarrow p\pi^0$	$\frac{\mathcal{B}_{\Lambda_c^+ \rightarrow p\pi^0}}{\mathcal{B}_{\Lambda_c^+ \rightarrow p\eta}}$
BESIII	1.24 ± 0.29	< 0.27	< 0.24
Sharma <i>et al</i> [3]	$0.2^a(1.7^b)$	0.2	$1.0^a(0.1^b)$
Uppal <i>et al</i> [4]	0.3	0.1-0.2	0.3-0.7
S. L. Chen <i>et al</i> [12]	...	0.11-0.36 ^c	...
Cai-Dian Lü <i>et al</i> [13]	...	0.45	...

^a assume positive sign of p-wave amplitude of $\Lambda_c^+ \rightarrow \Xi^0 K^+$

^b assume negative sign of p-wave amplitude of $\Lambda_c^+ \rightarrow \Xi^0 K^+$

^c calculated relying on different values of parameters b and α

The BESIII collaboration thanks the staff of BEPCII, the Institute of High Energy Physics (IHEP) computing center and the supercomputing center of University of Science and Technology of China (USTC) for their strong support. P. L. Li and H. P. Peng are grateful to Prof. Hai-Yang Cheng for enlightening discussions. This work is supported in part by National Key Basic Research Program of China under Contract No. 2015CB856700; National Natural Science Foundation of China (NSFC) under Contracts Nos. 11125525, 11235011, 11322544, 11335008, 11425524, 11625523, 11635010, 11375170, 11275189, 11475164, 11475169, 11605196, 11605198; the Chinese Academy of Sciences (CAS) Large-Scale Scientific Facility Program; the CAS Center for Excellence in Particle Physics (CCEPP); the Collaborative Innovation Center for Particles and Interactions (CICPI); Joint Large-Scale Scientific Facility Funds of the NSFC and CAS under Contracts Nos. U1232201, U1332201, U1532257, U1532258, U1532102; CAS under Contracts Nos. KJCX2-YW-N29, KJCX2-YW-N45, QYZDJ-SSW-SLH003; 100 Talents Program of CAS; National 1000 Talents Program of China; INPAC and Shanghai Key Laboratory for Particle Physics and Cosmology; German Research Foundation DFG under Contracts Nos. Collaborative Research Center CRC 1044, FOR 2359; Istituto Nazionale di Fisica Nucleare, Italy; Koninklijke Nederlandse Akademie van Wetenschappen (KNAW) under Contract No. 530-4CDP03; Ministry of Development of Turkey under Contract No. DPT2006K-120470; National Science and Technology fund; The Swedish Research Council; U. S. Department of Energy under Contracts Nos. DE-FG02-05ER41374, DE-SC-0010504, DE-SC-0010118, DE-SC-0012069; U.S. National Science Foundation; University of Groningen (RuG) and the Helmholtzzentrum fuer Schwerionenforschung GmbH (GSI), Darmstadt; WCU Program of National Research Foundation of Korea under Contract No. R32-2008-000-10155-0.

-
- [1] Y. Kohara, Nuovo Cim. A **111**, 67 (1998).
 - [2] M. A. Ivanov, J. G. Korner, V. E. Lyubovitskij, A. G. Rusetsky, Phys. Rev. D **57**, 5632 (1998).
 - [3] K. K. Sharma, R. C. Verma, Phys. Rev. D **55**, 7067 (1997).
 - [4] T. Uppal, R. C. Verna, M. P. Khanna, Phys. Rev. D **49**, 3417 (1994).
 - [5] P. Zenczykowski, Phys. Rev. D **50**, 402 (1994).
 - [6] J. G. Korner, M. Kramer, Z. Phys. C **55**, 659 (1992).
 - [7] L. L. Chau, H. Y. Cheng, B. Tseng, Phys. Rev. D **54**, 2132 (1996).
 - [8] G. S. Abrams *et al.* [MARKIII Collaboration], Phys. Rev. Lett. **44**, 10 (1980).
 - [9] A. M. Cnops *et al.* [BNL-0427 Collaboration], Phys. Rev. Lett. **42**, 197 (1979).
 - [10] C. Patrignani *et al.* [Particle Data Group], Chin. Phys. C **40**, 100001 (2016).

- [11] M. Ablikim *et al.* [BESIII Collaboration], Phys. Rev. Lett. **116**, 052001 (2016).
- [12] S. L. Chen, X. H. Guo, X. Q. Li and G. L. Wang, Commun. Theor. Phys. **40**, 563 (2003)
- [13] Cai-Dian Lü, Wei Wang, and Fu-Sheng Yu, Phys. Rev. D **93**, 056008 (2016).
- [14] M. Ablikim *et al.* [BESIII Collaboration], Chin. Phys. C **40**, 063001 (2016).
- [15] M. Ablikim *et al.* [BESIII Collaboration], Chin. Phys. C **39**, 093001 (2015).
- [16] M. Ablikim *et al.* [BESIII Collaboration], Nucl. Instrum. Meth. A **614**, 345 (2010).
- [17] J. Z. Bai *et al.* [BES Collaboration], Nucl. Instrum. Meth. A **344**, 319 (1994).
- [18] S. Agostinelli *et al.* [GEANT Collaboration], Nucl. Instrum. Meth. A **506**, 250 (2003).
- [19] J. Allison *et al.*, IEEE Trans. Nucl. Sci. **53**, 270 (2006).

- [20] Z. Y. Deng *et al.*, Chin. Phys. C **30**, 371 (2006).
- [21] S. Jadach, B. F. L. Ward, Z. Was, Phys. Rev. D **63**, 113009 (2001); Comput. Phys. Commun. **130**, 260 (2000).
- [22] R. G. Ping, Chin. Phys. C **32**, 599 (2008).
- [23] D. J. Lange, Nucl. Instrum. Meth. A **462**, 152 (2001).
- [24] J. C. Chen, G. S. Huang, X. R. Qi, D. H. Zhang and Y. S. Zhu, Phys. Rev. D **62**, 034003 (2000).
- [25] A. Drescher *et al.* [ARGUS Collaboration], Nucl. Instrum. Meth. A **237**, 464 (1985).
- [26] H. Albrecht *et al.* [ARGUS Collaboration], Phys. Rev. Lett. B **241**, 278 (1990).
- [27] M. R. Convery, Incorporating multiplicative systematic errors in branching ratio limits[R], SLAC-TN-03-001, 2003.
- [28] K. Stenson, A more exact solution for incorporating multiplicative systematic uncertainties in branching ratio limits, arXiv:physics/0605236 [physics.data-an].